Batch and fixed-bed column study for *p*-nitrophenol, methylene blue, and U(VI) removal by polyvinyl alcohol–graphene oxide macroporous hydrogel bead

Dan Chen, Jun Zhou, Hongyu Wang and Kai Yang

ABSTRACT

There is an increasing need to explore effective and clean approaches for hazardous contamination removal from wastewaters. In this work, a novel bead adsorbent, polyvinyl alcohol–graphene oxide (PVA-GO) macroporous hydrogel bead was prepared as filter media for *p*-nitrophenol (PNP), dye methylene blue (MB), and heavy metal U(VI) removal from aqueous solution. Batch and fixed-bed column experiments were carried out to evaluate the adsorption capacities of PNP, MB, and U(VI) on this bead. From batch experiments, the maximum adsorption capacities of PNP, MB, and U(VI) reached 347.87, 422.90, and 327.55 mg/g. From the fixed-bed column experiments, the adsorption capacities of PNP, MB, and U(VI) decreased with initial concentration increasing from 100 to 400 mg/L. The adsorption capacities of PNP, MB, and U(VI) decreased with increasing flow rate. Also, the maximum adsorption capacity of PNP decreased as pH increased from 3 to 9, while MB and U(VI) presented opposite tendencies. Furthermore, the bed depth service Time (BDST) model showed good linear relationships for the three ions' adsorption processes in this fixed-bed column, which indicated that the BDST model effectively evaluated and optimized the adsorption process of PVA-GO macroporous hydrogel bead in fixed-bed columns for hazardous contaminant removal from wastewaters.

Key words | bead, BDST model, fixed-bed column, graphene oxide, hazardous contaminants

Dan Chen
Jun Zhou
College of Urban Construction,
Nanjing Tech University,
Nanjing 211800,
China

Hongyu Wang (corresponding author)
Kai Yang
School of Civil Engineering,
Wuhan University,
Wuhan 430072,
China
E-mail: *hongyuwangcc@126.com*

INTRODUCTION

p-Nitrophenol (PNP) is widely used in numerous industries such as fungicides, pesticides, drugs, and explosives, so that it becomes one of the most common organic pollutants in industrial wastewaters (Zarei *et al.* 2015; Li *et al.* 2016a). Owing to its toxicity to human beings and microorganisms, high persistence in waters and non-biodegradation, lots of methods including chemical oxidation, biological degradation, and adsorption are used to remove PNP from waters (Nakatsuji *et al.* 2015; Pang & Lei 2016). Among these methods, adsorption is considered as one of the most promising approaches for PNP removal not only because this process takes less time than microbial degradation, but also it costs less than the oxidation method. Therefore, looking for an effective and economical adsorbent for PNP removal tends to be important.

Methylene blue (MB) as a typical cationic dye is commonly used in many fields such as printing, dyeing, textile, cosmetic, and leather (Agarwal *et al.* 2016; Liu *et al.* 2016). It is known to cause serious problems for human health and aquatic environments so that numerous methods such as precipitation, oxidation, membrane separation, photocatalytic degradation, and adsorption are carried out to remediate MB-contaminated wastewaters (Li *et al.* 2016a; Wong *et al.* 2016). In recent years, there has been increasing focus on investigating new and efficient adsorbents for MB removal from wastewaters, such as biochar, polymer, graphene oxide, metal oxide, and nanocomposite (Agarwal *et al.* 2016; Li *et al.* 2016a; Liu *et al.* 2016).

The radioactive waste U(VI) from nuclear industries often causes serious pollution in the water environment and even cause damages to human beings (Liu *et al.* 2014). Thus, it is of vital importance to explore efficient technology to removal U(VI) from subsurface environments. Numerous approaches have been focused on U(VI) removal from aqueous solutions, such as redox, co-precipitation, membrane processes, solvent extraction, cementation, and adsorption

doi: 10.2166/wst.2017.524

(Hu *et al.* 2016; Mahmoud 2016). Due to the high efficiency and low cost, adsorption is considered as one of the most popular methods for U(VI) removal. Therefore, many adsorbents, including graphene oxide, nanoporous alumina, and oxide nanopowder, are prepared for U(VI) removal (Cheng *et al.* 2015; Hu *et al.* 2016).

Nakatsuji and coworkers (Nakatsuji *et al.* 2015) used zero-valent iron for PNP removal and proved that zero-valent iron was efficient for PNP adsorption. In the study of Yang *et al.* (2015), nanosized hydrated ferric oxides were prepared for PNP removal and achieved satisfactory adsorption capacity. Li *et al.* (2016a) prepared wheat straw biochar for MB adsorption, and demonstrated that wheat straw biochar could be used for effective MB removal when assisted by an external magnetic field. El-Mekkawi and coworkers (El-Mekkawi *et al.* 2016) used zeolites as adsorbent for MB removal and obtained good results. Liu and coworkers (Liu *et al.* 2014) prepared hierarchical $Fe_4(P_2O_7)_3$ for U(VI) removal and demonstrated that $Fe_4(P_2O_7)_3$ could be an ideal adsorbent for U(VI) removal from aqueous environment. Mahmoud (2016) used oxide nanopowder for U(VI) adsorption, and indicated that this adsorbent exhibited excellent U(VI) removal capacity and had a good selectivity for U(VI) adsorption from aqueous solution.

Graphene oxide (GO) exhibits excellent affinity to many pollutants in water because of its abundant functional groups, large specific surface area, and high adsorption capacity (Gong *et al.* 2015). However, GO is not easy to be collected in the treated water and then will bring about secondary pollution. In the present study, polyvinyl alcohol–graphene oxide (PVA-GO) macroporous hydrogel bead is prepared as filter media to remove PNP, MB, and U(VI) in a fixed-bed column. A series of experiments is carried out to investigate the parameters of initial concentration, flow rate, and pH.

MATERIALS AND METHODS

Chemicals and regents

All chemicals and reagents used in this experiment were analytical grade. In addition, 3-aminopropyltriethoxysilane ($C_9H_{23}NO_3Si$), hydrochloric acid (HCl), sodium hydroxide (NaOH), sulfuric acid (H_2SO_4), phosphoric acid (H_3PO_4), graphite powder, potassium permanganate ($KMnO_4$), hydrogen peroxide (H_2O_2), ethanol (C_2H_6O), sodium nitrite ($NaNO_2$), acetone (CH_3COCH_3), PVA ((C_2H_4O)n), sodium alginate (($C_6H_7NaO_6$)x), calcium chloride ($CaCl_2$), boric acid (H_3BO_3), sodium chloride (NaCl), calcium carbonate ($CaCO_3$), PNP, MB, and uranium nitrate ($UO_2(NO_3)_2{\cdot}6H_2O$) were purchased from Aladdin and Qiangsong Fine Chemicals.

Adsorbent preparation

The preparation method of 3-aminopropyltriethoxysilane-modified GO was according to our previous study (Chen *et al.* 2016). For obtaining PVA-modified GO hydrogel beads, 32.4 g PVA, 10 g sodium alginate, and 54 g calcium carbonate were added to 600 mL deionized water, and then stirred under 95 °C condition until dissolved. Then 5 g 3-aminopropyltriethoxysilane-modified GO was added to the mixture and the mixture was stirred for 8 h under 80 °C condition. Afterwards, the mixture was dropwise added to 5% $CaCl_2$-saturated boric acid solution by an injector. After 48 h, the beads were soaked in 1 M HCl solution until bubbles had disappeared. At last, PVA-modified GO macroporous hydrogel beads were obtained.

SEM and XPS analyses

Surface morphology of the samples was determined using scanning electron microscopy (SEM) (ZEISS, Germany). X-ray diffraction (XRD) spectra were determined using the X-ray diffractometer X'Pert Pro, PANalytical. X-ray photoelectron spectroscopy (XPS) spectra were measured by a Thermo Fisher ESCALAB 250Xi.

Batch adsorption experiments

In order to control quality, all the isotherm experiments were conducted in duplicate and the differences between the two measurements were lower than 3%. Batch adsorption isotherm experiments of PNP, MB, and U(VI) adsorption on PVA-GO macroporous hydrogel beads were carried out by adding 0.05 g (dry weight) of each adsorbent to 200 mL Erlenmeyer flasks containing 100 mL PNP, MB, and U(VI) solution at 25 °C in a mechanical shaker. The concentration of PNP, MB, and U(VI) varied from 5 to 500 mg/L. After 24 h reaction, the samples were taken, and the PNP, MB, and U(VI) contents were determined by the standard method (PNP and MB were detected by UV spectrophotometer at the maximum absorbance wavelengths at 317 nm and 662 nm, U(VI) was measured using the arsenazo III spectrophotometric method at 650 nm). Control samples containing all other reagents except adsorbent were also analyzed. The PNP, MB, and U(VI)

adsorption data were fitted to the simple Langmuir and Freundlich equations.

Column experiments and data analysis

The fixed-bed column experiments were carried out in a glass column (diameter 5 cm, length 15 cm). The whole column was filled with PVA-modified GO macroporous hydrogel beads. The influent was pumped from the bottom to the top by a pump. The initial concentrations of PNP, MB, and U(VI) varied from 100 to 400 mg/L. The flow rates increased from 1 to 4 mL/min, and pH varied from 3 to 9.

When the effluent concentration reaches 0.1% of the influent concentration, the breakthrough point is arrived, and the time is breakthrough time (t_b). Also, when the effluent concentration reaches 95% of the influent concentration, the exhaustion point is arrived, and the time is exhaustion time (t_e).

The total adsorption capacity q_{total} (mg) is calculated by Equation (1):

$$q_{total} = \frac{QA}{1000} = \frac{Q}{1000}\int_{t=0}^{t=t_{total}} C_{ad}dt \quad (1)$$

where Q is the flow rate (mL/min), A is the area above the breakthrough curve (C_t/C_0 as vertical axis, time as horizontal axis; C_t is the effluent concentration, C_0 is the influent concentration), t_{total} is the total flow time (min), and C_{ad} is the adsorbed concentration (mg/L).

The maximum adsorption capacity q (mg/g) of the column is calculated by Equation (2):

$$q = \frac{q_{total}}{m} \quad (2)$$

where m is the adsorbent dry weight (g).

Mathematical models

The Freundlich model (Equation (3)) and Langmuir model (Equation (4)) were used to evaluate the adsorption capacities of PNP, MB, and U(VI) adsorption on PVA-GO macroporous hydrogel bead:

$$\ln q_e = \ln K_F + \frac{1}{n}\ln C_e \quad (3)$$

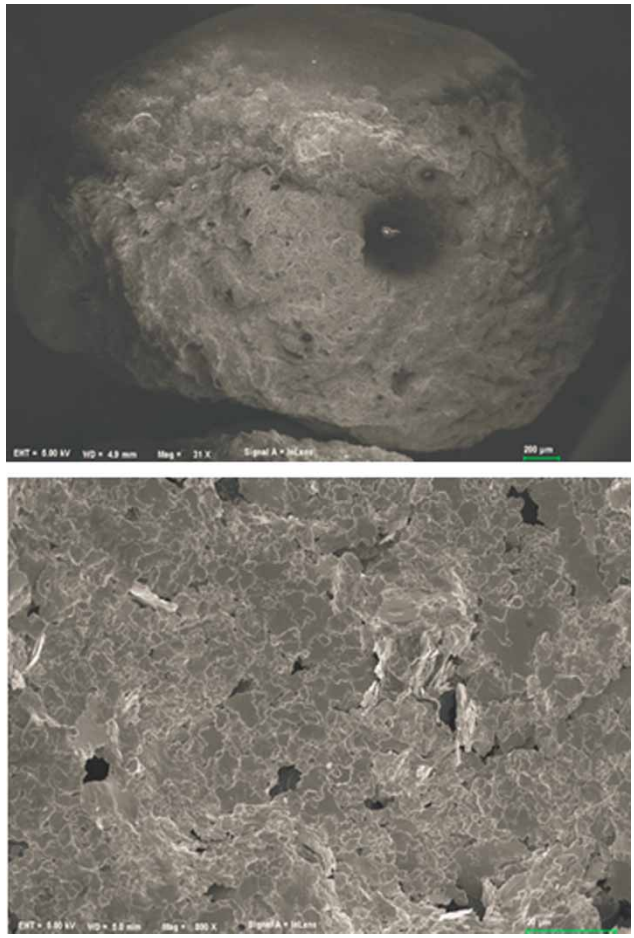

Figure 1 | SEM images of PVA-GO macroporous hydrogel bead.

$$\frac{C_e}{q_E} = \frac{C_e}{q_{\max}} + \frac{1}{K_L q_{\max}} \quad (4)$$

where q_e is the equilibrium adsorption capacity (mg/g), C_e is the equilibrium concentration (mg/L), K_F and $1/n$ are

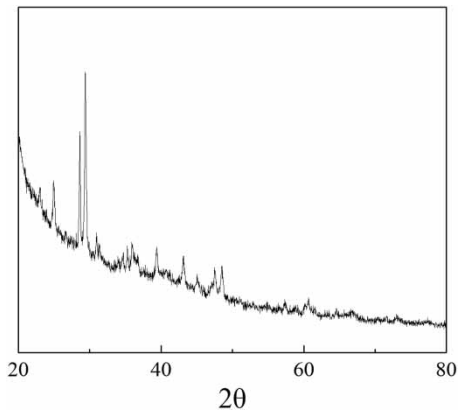

Figure 2 | XRD patterns of PVA-GO macroporous hydrogel bead.

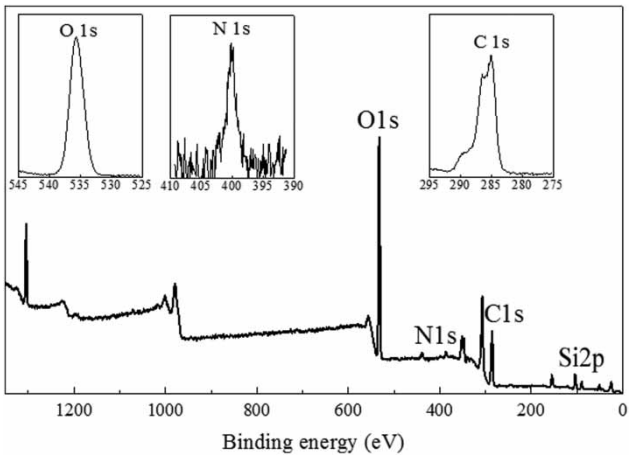

Figure 3 | XPS spectrum of PVA-GO macroporous hydrogel bead.

Freundlich isotherm constants, q_{max} is the maximum adsorption capacity (mg/g), and K_L is the adsorption constant (L/mg).

The bed depth service time (BDST) model (Equation (5)) was used to evaluate the relationship between adsorbent amount and service time:

$$t = \frac{N_0}{C_0 v} H - \frac{1}{k C_0} \ln\left(\frac{C_0}{C_t} - 1\right) \quad (5)$$

where t is the service time (min), N_0 is the dynamic adsorption capacity (mg/L), v is the linear flow velocity of feed (cm/min), H is the height of the adsorbent (cm), and k is the adsorption rate constant (L/(mg·min)).

RESULTS AND DISCUSSION

Characterization of PVA-GO macroporous hydrogel bead

SEM images of PVA-GO macroporous hydrogel bead are shown in Figure 1. It is obvious that the surfaces of the bead were quite rough, which provided sufficient surface areas for adsorption. In addition, there were many pore structures on the bead surfaces that could not only increase the surface areas, but also increase the sorption sites, thus

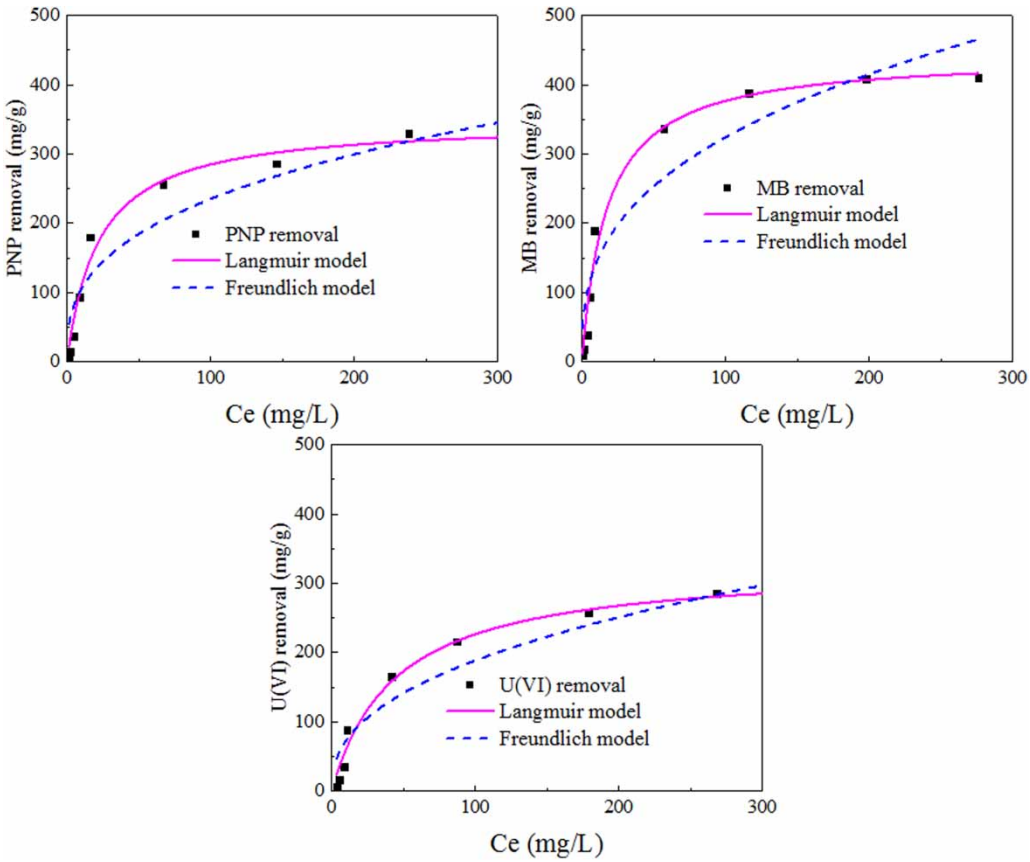

Figure 4 | Langmuir and Freundlich equations fitted to PNP, MB, and U(VI) adsorption data.

Table 1 | Estimated isotherm parameters for PNP, MB, and U(VI) adsorption on PVA-GO macroporous hydrogel bead

	Freundlich model			Langmuir model		
Adsorbate	K_F	$1/n$	R^2	q_{max}	K_L	R^2
PNP	46.90	0.3490	0.8876	347.87	0.0451	0.9801
MB	62.86	0.3560	0.9022	442.90	0.0568	0.9847
U(VI)	27.90	0.4100	0.9110	327.55	0.0223	0.9828

promoting the adsorption abilities. The XRD pattern of PVA-GO macroporous hydrogel bead is displayed in Figure 2. There were two obvious peaks at $2\theta \approx 24.5°$ and $2\theta \approx 28.5°$, which were ascribed to the crystalline structure of PVA. In fact, sodium alginate and GO did not present peaks on the XRD pattern of the macroporous hydrogel bead, which demonstrated that the materials exhibited good compatibility in the synthetic macroporous hydrogel bead. Figure 3 shows the XPS spectrum of PVA-GO macroporous hydrogel bead. The binding energy illustrated that O 1 s, C 1 s, N 1 s, and Si 2p were the main elements on the PVA-GO macroporous hydrogel bead surface. The observed N and Si elements demonstrated that -NH_2 existed on the bead, so that the hydrogel bead exhibited larger adsorption abilities for contaminants.

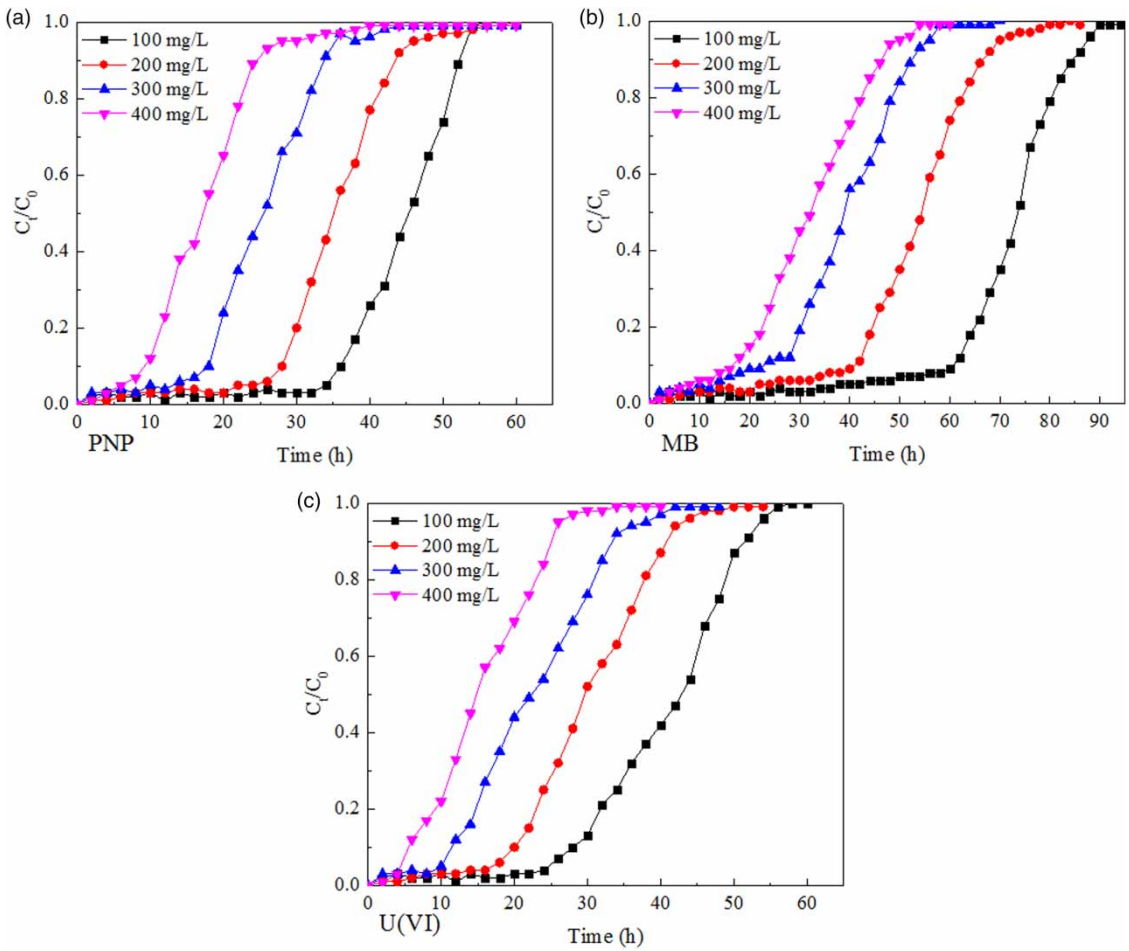

Figure 5 | Breakthrough curves of PNP, MB, and U(VI) adsorption on PVA-GO macroporous hydrogel bead at different initial concentrations.

Adsorption isotherms of batch experiments

The batch adsorption data of PNP, MB, and U(VI) adsorption on PVA-GO macroporous hydrogel bead were fitted to Langmuir and Freundlich equations (Figure 4). The calculated isotherm parameters of the Freundlich model and Langmuir model for PNP, MB, and U(VI) adsorption on PVA-GO macroporous hydrogel bead are presented in Table 1. In general, the Langmuir model better fitted the batch adsorption data of PNP, MB, and U(VI) adsorption than the Freundlich model, which indicated that the adsorption processes of PNP, MB, and U(VI) on PVA-GO macroporous hydrogel beads were mainly controlled by the monolayer adsorption mechanism. According to the Langmuir model, the maximum adsorption capacities of PNP, MB, and U(VI) were 347.87, 422.90, and 327.55 mg/g, which were much greater than found in similar researches (Zhang *et al.* 2015; Li *et al.* 2016c; Mahmoud 2016). Based on the batch adsorption experiments, it could be concluded that the PVA-GO macroporous hydrogel bead was an effective and promising adsorbent for PNP, MB, and U(VI) removal from wastewaters.

Effect of initial concentration in columns

The effects of initial concentration of PNP, MB, and U(VI) adsorption on PVA-GO macroporous hydrogel bead in fixed-bed column were investigated at pH 7, flow rate 1 mL/min with initial concentration varied from 100 to 400 mg/L. The breakthrough curves are given in Figure 5(a)–5(c), and the calculated parameters are displayed in Table 2. It is obvious that the adsorption capacities of PNP, MB, and U(VI) showed increased trends while the exhaustion times decreased with increasing initial concentration. For PNP adsorption, the exhaustion time decreased from 54 to 28 h, while the maximum adsorption capacity increased from 0.66 to 1.30 mg/g with initial PNP concentration increasing from 100 to 400 mg/L. For MB adsorption, when initial MB concentration increased from 100 to 400 mg/L, the maximum adsorption capacity increased from 0.92 to 1.62 mg/g, while the exhaustion time decreased from 88 to 48 h. For U(VI) adsorption, the maximum adsorption capacity increased from 0.51 to 1.41 mg/g, and the exhaustion time decreased from 52 to 28 h when initial U(VI) concentration increased from 100 to 400 mg/L. When there were more PNP, MB, and U(VI) ions present in the fixed-bed column, the ions were more easily adsorbed onto PVA-GO macroporous hydrogel beads, so that the exhaustion time decreased. In addition, the driving force for the mass transfer during the adsorption process controlled the adsorption capacity in the column. Some researchers reported that high initial concentration would facilitate the driving force for the mass transfer in the fixed-bed column so that the ultimate adsorption capacity increased (Ataei-Germi & Nematollahzadeh 2016; Han *et al.* 2009a). In the present study, more PNP, MB, and U(VI) ions fast contacted with the macroporous hydrogel beads and occupied the adsorption sites, improving the driving force for the mass transfer, so that the PNP, MB, and U(VI) adsorption capacities showed obvious increases.

Table 2 | Parameters obtained from the breakthrough data at various operational conditions

Ion	C_0 (mg/L)	Q (mL/min)	pH	t_e (h)	q_{total} (mg)	q (mg/g)
PNP	100	1	7	54	13.14	0.66
	200	1	7	46	19.76	0.99
	300	1	7	36	24.48	1.22
	400	1	7	28	25.92	1.30
	100	1	7	56	13.09	0.65
	100	2	7	52	8.17	0.41
	100	3	7	42	3.39	0.17
	100	4	7	30	1.83	0.09
	100	1	3	76	37.58	1.88
	100	1	5	66	23.06	1.15
	100	1	7	54	12.85	0.64
	100	1	9	30	5.49	0.27
MB	100	1	7	88	18.34	0.92
	200	1	7	70	24.94	1.25
	300	1	7	56	31.23	1.56
	400	1	7	48	32.34	1.62
	100	1	7	86	18.76	0.94
	100	2	7	80	13.45	0.67
	100	3	7	68	7.58	0.38
	100	4	7	52	2.34	0.12
	100	1	3	46	3.25	0.16
	100	1	5	62	10.93	0.55
	100	1	7	88	17.98	0.90
	100	1	9	98	42.21	2.11
U(VI)	100	1	7	52	10.13	0.51
	200	1	7	42	21.35	1.07
	300	1	7	36	26.72	1.34
	400	1	7	26	28.15	1.41
	100	1	7	52	10.16	0.51
	100	2	7	46	5.98	0.30
	100	3	7	38	2.41	0.12
	100	4	7	28	1.06	0.05
	100	1	3	26	2.75	0.14
	100	1	5	36	6.33	0.32
	100	1	7	52	10.37	0.52
	100	1	9	62	22.84	1.14

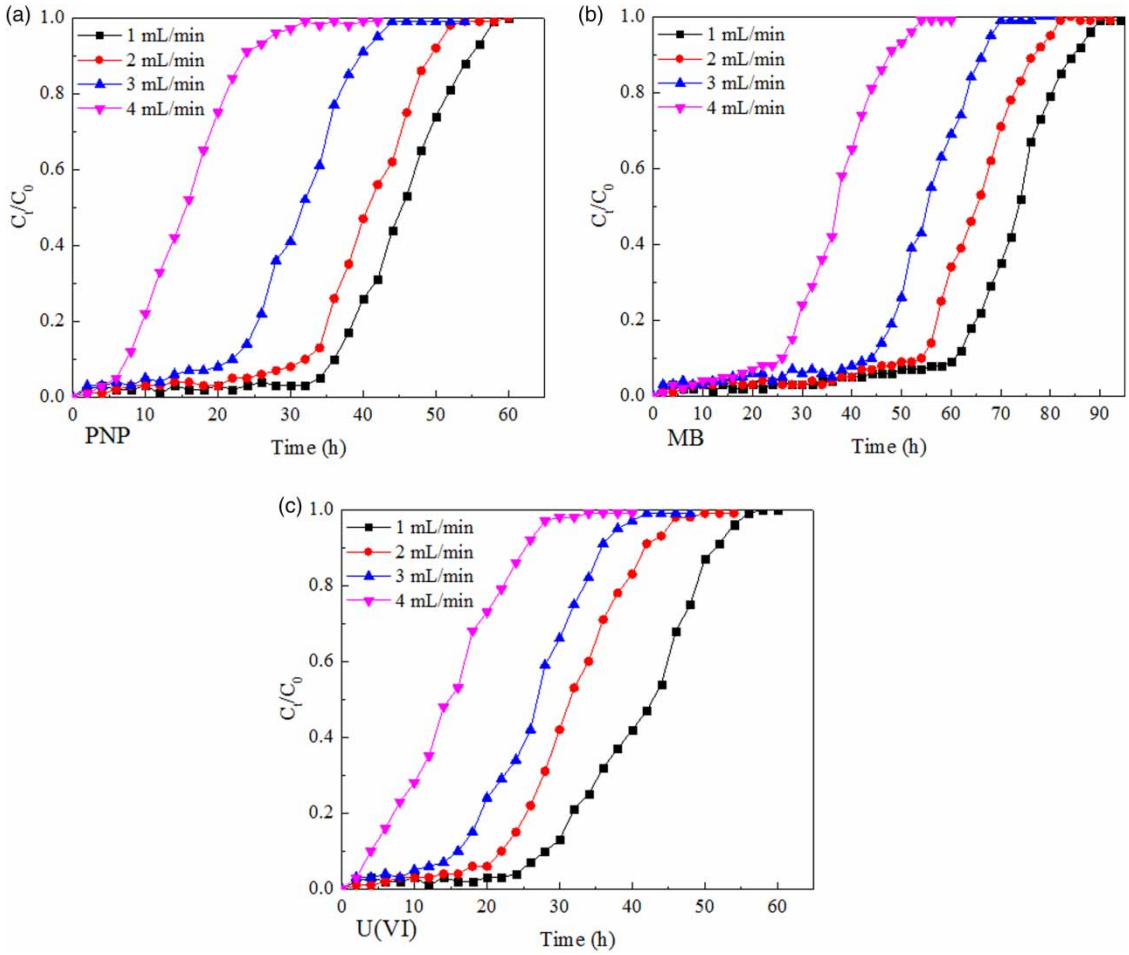

Figure 6 | Breakthrough curves of PNP, MB, and U(VI) adsorption on PVA-GO macroporous hydrogel bead at different flow rates.

Effect of flow rate in columns

The effects of flow rate on PNP, MB, and U(VI) adsorption on PVA-GO macroporous hydrogel bead in fixed-bed column were investigated at pH 7, initial concentration 100 mg/L with flow rate increasing from 1 to 4 mL/min. The breakthrough curves are given in Figure 6(a)–6(c), and the calculated parameters are displayed in Table 2. Generally, the exhaustion time and maximum adsorption capacity both decreased with increased flow rate in this fixed-bed column. For PNP adsorption, the exhaustion time decreased from 56 to 30 h and the maximum adsorption capacity decreased from 0.65 to 0.09 mg/g with flow rate increasing from 1 to 4 mL/min. For MB adsorption, when flow rate increased from 1 to 4 mL/min, the maximum adsorption capacity decreased from 0.94 to 0.12 mg/g and the exhaustion time decreased from 86 to 52 h. For U(VI) adsorption, the exhaustion time decreased from 52 to 28 h and the maximum adsorption capacity decreased from 0.51 to 0.05 mg/g when flow rate increased from 1 to 4 mL/min. When flow rate increased, there were more PNP, MB, and U(VI) ions rapidly contacted with the macroporous hydrogel bead, so that the breakthrough and exhaustion times were reached earlier (Gong *et al.* 2015; Ataei-Germi & Nematollahzadeh 2016). Moreover, the turbulence of the flow increased with increased flow rate, and the residence time decreased under high flow rate condition (Han *et al.* 2009b; Uddin *et al.* 2009). Because of this the adsorption capacities of PNP, MB, and U(VI) onto PVA-GO macroporous hydrogel bead decreased as flow rate increased from 1 to 4 mL/min in this fixed-bed column.

Effect of pH in columns

The effects of pH on PNP, MB, and U(VI) adsorption on PVA-GO macroporous hydrogel bead in fixed-bed column were investigated at initial concentration 100 mg/L, flow rate 1 mL/min with pH increasing from 3 to 9. The

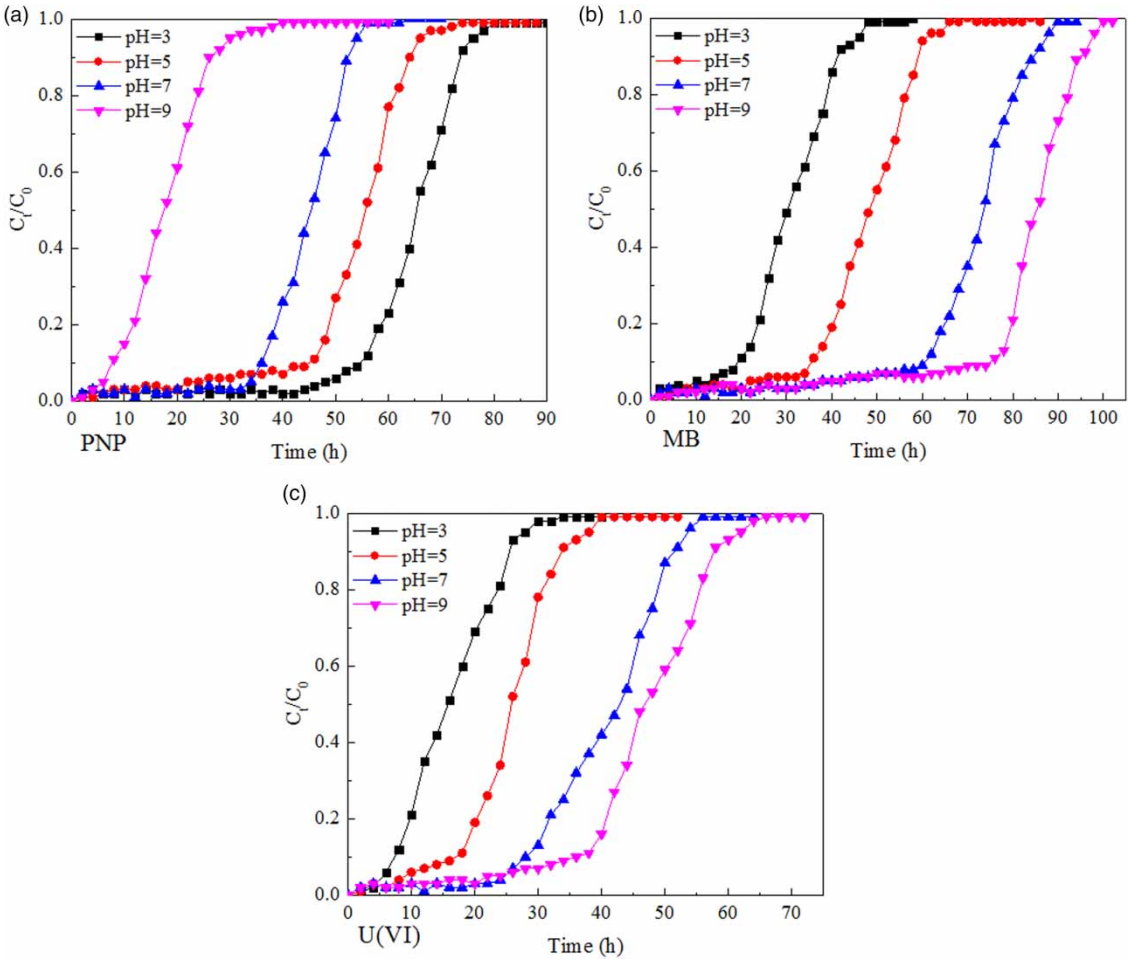

Figure 7 | Breakthrough curves of PNP, MB, and U(VI) adsorption on PVA-GO macroporous hydrogel bead at different pH.

breakthrough curves are given in Figure 7(a)–7(c), and the calculated parameters are displayed in Table 2. For PNP adsorption, the exhaustion time decreased from 76 to 30 h and the maximum adsorption capacity decreased from 1.88 to 0.27 mg/g as pH increased from 3 to 9. For MB adsorption, when pH increased from 3 to 9, the maximum adsorption capacity increased from 0.16 to 2.11 mg/g, and the exhaustion time increased from 46 to 98 h. For U(VI) adsorption, the exhaustion time increased from 26 to 62 h, and the maximum adsorption capacity increased from 0.14 to 1.14 mg/g. For PNP, the decreasing adsorption capacity with increasing pH condition was because the surface of the macroporous hydrogel bead was more negatively charged under increasing pH environment, so the negatively charged sites on PVA-GO macroporous hydrogel beads do not favor the PNP adsorption process due to electrostatic repulsion (Zhang *et al.* 2015). In addition, under acid environment, more H^+ would complete with MB and U(VI) ions for available sorption sites on PVA-GO macroporous hydrogel beads (Hu *et al.* 2016; Li *et al.* 2016b), so that the adsorption capacities of MB and U(VI) ions decreased under acid condition. However, because the surfaces of PVA-GO macroporous hydrogel beads were more negatively charged under alkaline environment, the adsorption capacities of positive ions of MB and U(VI) both increased significantly with increasing pH condition in this fixed-bed column. As a result, the considerable adsorption capacities of PNP, MB, and U(VI) on PVA-GO macroporous hydrogel bead demonstrated that PVA-GO macroporous hydrogel bead was effective for PNP, MB, and U(VI) removal in fixed-bed column.

BDST model results for column experiments

The BDST model was always used to reveal the relationship between service time and the amount of adsorbent in

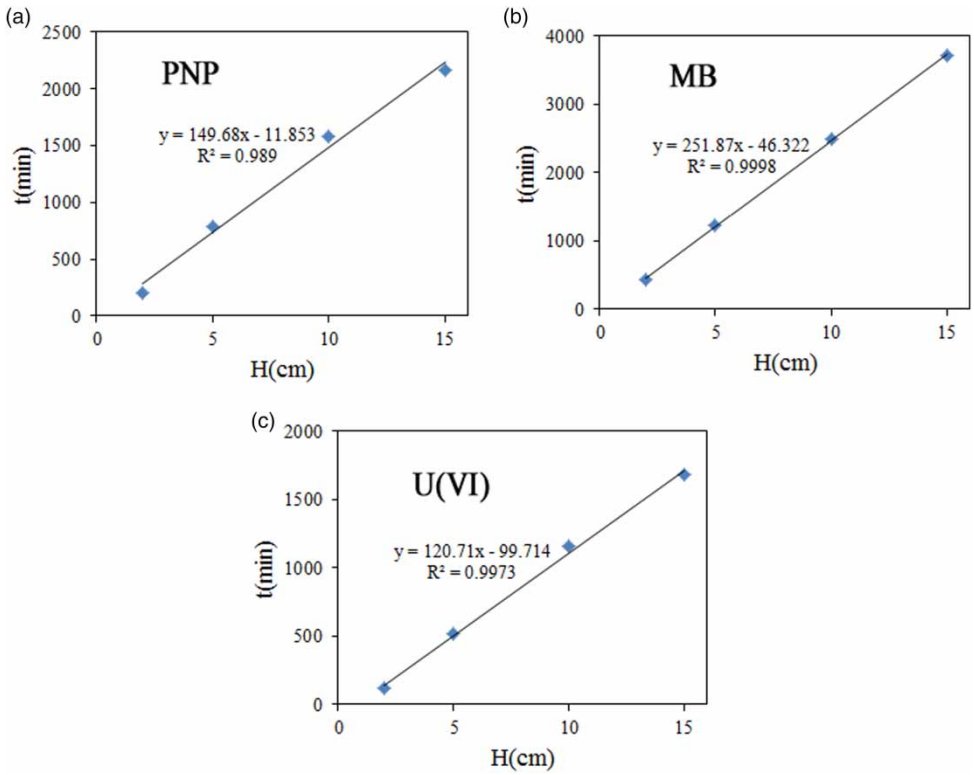

Figure 8 | BDST model of PNP, MB, and U(VI) adsorption on PVA-GO macroporous hydrogel bead (initial concentration100 mg/L, flow rate 1 mL/min, pH 7).

fixed-bed column experiments (Maji *et al.* 2007; Uddin *et al.* 2009; Wang *et al.* 2016). Figure 8 displays the BDST model results of PNP, MB, and U(VI) adsorption on PVA-GO macroporous hydrogel bead in the fixed-bed column, and the calculated parameters are shown in Table 3. Overall, the BDST model showed good linear relationships ($R^2 > 0.98$) for the three ions' adsorption process in this fixed-bed column, which indicated that PVA-GO macroporous hydrogel bead was an effective filter media for PNP, MB, and U(VI) removal in a fixed-bed column. Specifically, the adsorption data of MB ($R^2 = 0.999$) and U(VI) ($R^2 = 0.997$) were better fitted to the BDST model than PNP ($R^2 = 0.989$) adsorption, suggesting that the PVA-GO macroporous hydrogel bead exhibited better adsorption abilities for MB and U(VI) than for PNP. Based on the BDST model analyses, it could be concluded that the BDST model can be effectively used to evaluate and optimize the adsorption process of PVA-GO macroporous hydrogel bead in fixed-bed columns for removal of dye, heavy metal and some other hazardous contaminants from wastewaters.

Table 3 | BDST model parameters

Adsorbate	N_0 (mg/L)	k (L/(mg·min))	R^2
PNP	762.77	0.0039	0.989
MB	1,283.53	0.0010	0.999
U(VI)	615.14	0.0005	0.997

CONCLUSIONS

The PVA-GO macroporous hydrogel bead showed strong affinity for PNP, MB, and U(VI) ions with Langmuir maximum adsorption capacities of 347.87, 422.90, and 327.55 mg/g, indicating that the PVA-GO macroporous hydrogel bead exhibited high-efficiency adsorption abilities for PNP, MB, and U(VI). The BDST model well described the three ions' adsorption process in this fixed-bed column ($R^2 > 0.98$), which also demonstrated that PVA-GO macroporous hydrogel bead was an effective filter media for PNP, MB, and U(VI) removal in a fixed-bed column. Findings of this study indicated that the PVA-GO macroporous hydrogel bead was an effective and promising adsorbent that can be used as filter media for PNP, MB, and U(VI) removal in a fixed-bed column.

ACKNOWLEDGEMENTS

This work was financially supported by the National Natural Science Foundation of China (NSFC) (51378400) and the National Science and Technology Pillar Program (2014BAL04B04).

REFERENCES

Agarwal, S., Sadegh, H., Monajjemi, M., Hamdy, A. S., Ali, G. A. M., Memar, A. O. H., Shahryari-ghoshekandi, R., Tyagi, I. & Gupta, V. K. 2016 Efficient removal of toxic bromothymol blue and methylene blue from wastewater by polyvinyl alcohol. *J. Mol. Liq.* **218**, 191–197.

Ataei-Germi, T. & Nematollahzadeh, A. 2016 Bimodal porous silica microspheres decorated with polydopamine nanoparticles for the adsorption of methylene blue in fixed-bed columns. *J. Colloid Interf. Sci.* **470**, 172–182.

Chen, D., Zhang, H., Yang, K. & Wang, H. 2016 Functionalization of 4-aminothiophenol and 3-aminopropyltriethoxysilane with graphene oxide for potential dye and copper removal. *J. Hazard. Mater.* **310**, 179–187.

Cheng, W. C., Ding, C. C., Sun, Y. B. & Wang, X. K. 2015 Fabrication of fungus/attapulgite composites and their removal of U(VI) from aqueous solution. *Chem. Eng. J.* **269**, 1–8.

El-Mekkawi, D. M., Ibrahim, F. A. & Selim, M. M. 2016 Removal of methylene blue from water using zeolites prepared from Egyptian kaolins collected from different sources. *J. Environ. Chem. Eng.* **4**, 1417–1422.

Gong, J. L., Zhang, Y. L., Jiang, Y., Zeng, G. M., Cui, Z. H., Liu, K., Deng, C. H., Niu, Q. Y., Deng, J. H. & Huan, S. Y. 2015 Continuous adsorption of Pb(II) and methylene blue by engineered graphite oxide coated sand in fixed-bed column. *Appl. Surf. Sci.* **330**, 148–157.

Han, R. P., Wang, Y., Zhao, X., Wang, Y. F., Xie, F. L., Cheng, J. M. & Tang, M. S. 2009a Adsorption of methylene blue by phoenix tree leaf powder in a fixed-bed column: experiments and prediction of breakthrough curves. *Desalination* **245**, 284–297.

Han, R. P., Zou, L. N., Zhao, X., Xu, Y. F., Xu, F., Li, Y. L. & Wang, Y. 2009b Characterization and properties of iron oxide-coated zeolite as adsorbent for removal of copper(II) from solution in fixed bed column. *Chem. Eng. J.* **149**, 123–131.

Hu, T., Ding, S. & Deng, H. 2016 Application of three surface complexation models on U(VI) adsorption onto graphene oxide. *Chem. Eng. J.* **289**, 270–276.

Li, G., Zhu, W., Zhang, C., Zhang, S., Liu, L., Zhu, L. & Zhao, W. 2016a Effect of a magnetic field on the adsorptive removal of methylene blue onto wheat straw biochar. *Bioresour. Technol.* **206**, 16–22.

Li, L., Chen, L., Shi, H., Chen, X. & Lin, W. 2016b Evaluation of mesoporous bioactive glass (MBG) as adsorbent for removal of methylene blue (MB) from aqueous solution. *J. Environ. Chem. Eng.* **4**, 1451–1459.

Li, L., Liu, F., Duan, H., Wang, X., Li, J., Wang, Y. & Luo, C. 2016c The preparation of novel adsorbent materials with efficient adsorption performance for both chromium and methylene blue. *Colloids Surf. B* **141**, 253–259.

Liu, X., Xu, Y., Jin, R., Yin, P., Sun, L., Liang, T. & Gao, S. 2014 Facile synthesis of hierarchical $Fe_4(P_2O_7)_3$ for removal of U(VI). *J. Mol. Liq.* **200**, 311–318.

Liu, F., Zou, H. L., Hu, J. W., Liu, H. B., Peng, J. B., Chen, Y. W., Lu, F. H. & Huo, Y. P. 2016 Fast removal of methylene blue from aqueous solution using porous soy protein isolate based composite beads. *Chem. Eng. J.* **287**, 410–418.

Mahmoud, M. A. 2016 Kinetics and thermodynamics of U(VI) ions from aqueous solution using oxide nanopowder. *Process Saf. Environ.* **102**, 44–53.

Maji, S. K., Pala, A., Pal, T. & Adak, A. 2007 Modeling and fixed bed column adsorption of As(III) on laterite soil. *Sep. Purif. Technol.* **56**, 284–290.

Nakatsuji, Y., Salehi, Z. & Kawase, Y. 2015 Mechanisms for removal of *p*-nitrophenol from aqueous solution using zero-valent iron. *J. Environ. Manage.* **152**, 183–191.

Pang, Y. X. & Lei, H. Y. 2016 Degradation of p-nitrophenol through microwave-assisted heterogeneous activation of peroxymonosulfate by manganese ferrite. *Chem. Eng. J.* **287**, 585–592.

Uddin, M. T., Rukanuzzaman, M., Khan, M. M. & Islam, M. A. 2009 Adsorption of methylene blue from aqueous solution by jackfruit (*Artocarpus heterophyllus*) leaf powder: a fixed-bed column study. *J. Environ. Manage.* **90**, 3443–3450.

Wang, D., Chen, N., Yu, Y., Hu, W. & Feng, C. 2016 Investigation on the adsorption of phosphorus by Fe-loaded ceramic adsorbent. *J. Colloid Interf. Sci.* **464**, 277–284.

Wong, K. T., Eu, N. C., Ibrahim, S., Kim, H., Yoon, Y. & Jang, M. 2016 Recyclable magnetite-loaded palm shell-waste based activated carbon for the effective removal of methylene blue from aqueous solution. *J. Clean. Prod.* **115**, 337–342.

Yang, W. L., Yu, Z., Pan, B. C., Lv, L. & Zhang, W. M. 2015 Simultaneous organic/inorganic removal from water using a new nanocomposite adsorbent: a case study of *p*-nitrophenol and phosphate. *Chem. Eng. J.* **268**, 399–407.

Zarei, A. R., Rezaeivahidian, H. & Soleymani, A. R. 2015 Investigation on removal of p-nitrophenol using a hybridized photo-thermal activated persulfate process: central composite design modeling. *Process Saf. Environ.* **98**, 109–115.

Zhang, B., Li, F., Wu, T., Sun, D. J. & Li, Y. J. 2015 Adsorption of p-nitrophenol from aqueous solutions using nanographite oxide. *Colloids Surf. A* **464**, 78–88.

First received 5 July 2017; accepted in revised form 25 September 2017. Available online 11 October 2017